

Mariia Liaskovska^{1,2}, Tetiana Tatarchuk³, Volodymyr Kotsyubynsky⁴, Hanna Ersteniuk²

Zn-doped CoFe₂O₄ Nanoparticles Synthesized Using Ginkgo Biloba Extract: Cation Distribution, Mossbauer Studies and Application for Water Treatment

¹ Department of Chemistry, Vasyl Stefanyk Precarpathian National University, 57, Shevchenko Str., Ivano-Frankivsk, 76018, Ukraine, liaskovskam@gmail.com

² Department of H.O. Babenko Biological and Medical Chemistry, Ivano-Frankivsk National Medical University, 2, Halytska Str., Ivano-Frankivsk, 76018, Ukraine,

³ Educational and Scientific Center of Materials Science and Nanotechnology, Vasyl Stefanyk Precarpathian National University, 201, Galytska Str., Ivano-Frankivsk, Ukraine tatarchuk.tetyana@gmail.com

⁴ Department of Material Science and New Technology, Vasyl Stefanyk Precarpathian National University, 57, Shevchenko Str., Ivano-Frankivsk, 76018, Ukraine, kotsyubynsky@gmail.com

The cobalt-zinc ferrites Zn_{1-x}Co_xFe₂O₄ (where x=0; 0.2; 0.4; 0.6; 0.8; 1.0) were obtained by green synthesis using Ginkgo Biloba extract as reductant and fuel. The cation distribution of the spinel ferrites has been investigated by means of X-ray diffraction and Mossbauer spectroscopy. The surface morphology and elemental composition were analyzed by SEM and EDS. The crystallite size decrease with increasing Co²⁺ content calculated from Scherrer equation and Williamson-Hall method. Adsorption properties of the spinel system were investigated using Congo Red (CR) dye as model pollutant. It is concluded that the adsorption of Congo red dye molecules can occur due to electrostatic and donor-acceptor interactions with the adsorbent surface containing various amount of active centers.

Keywords: cobalt ferrite; spinel; green synthesis; adsorption; dye.

Received 18 September 2021; Accepted 20 December 2021.

Introduction

Currently, nanoparticles attract great interest due to their unique magnetic [1,2], optical [3], electrical [3], adsorption and catalytic [4] properties. The latest technologies are focused on the use of cheap, eco-friendly effective materials. Spinel nanoparticles may exhibit different sizes depending on synthesis method. Also, they can be used as adsorbents, pigments [5], catalysts [6], [7] and refractory materials. In order to synthesize spinels with high surface area and useful properties, different wet chemistry techniques have been attempted such as co-precipitation [8–10], hydrothermal method [4,6,11,12], sol-gel method [13–16], sonochemical method [6], ultrasound irradiation etc. Usually, different fuel agents are used such as citric acid,

benzyl alcohol, polyvinyl alcohol, ethylene glycol [17–20], which act as ligands and reactants during the synthesis for sol-gel synthesis of spinel NPs.

Green chemistry is considered as one of the promising techniques applied for nanoparticles synthesis and involves the using of the non-toxic plant extracts as effective reducing agent. To the best authors knowledge, although the plant extracts has been used to prepare Ag-NPs [21], Au-NPs [22] and spinel oxides [23]: NiFe₂O₄ [24], CuFe₂O₄ [25], CoFe₂O₄ [26,27] etc.

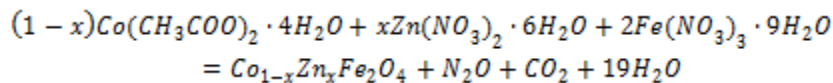
Ginkgo Biloba is one of the green sources of reductants [28]. The leaves of *Ginkgo Biloba* have a rich chemical composition. The leaf contains ginkgetin, campferol, quercetin, bilobetin and several other flavonoids; nonacosane, hexacosanol, amentoflavone, pinite; shikimova, quinine, linolenic and hydro-ginkolova

acids; terpenes, catechins, lactones, starch, wax, pentosan, mannan, β -sitosterol, essential and fatty oils[29].

The goal of this work is to synthesize magnetic Zn-doped cobalt ferrites with the general formula of Co_{1-x}Zn_xFe₂O₄ (0 ≤ x ≤ 1.0 with step 0.2) using *Ginkgo Biloba* leaf extract as eco-friendly fuel agent. Cobalt-zinc ferrite nanoparticles could be used for magnetic hyperthermia application, as carriers for drug delivery and as magnetic adsorbents. The aim of this work is also to establish the nature of the interaction of the cobalt-zinc ferrite surface with Congo Red dye molecules, as well as to determine the adsorption capacity of the spinel magnetic adsorbents.

I. Experimental

1.1. Green synthesis



Initially, the mixture of metal salts was dissolved in 50 ml of distilled water. The solutions have been then mixed for 30 min at a temperature of 45°C. 50 ml of the *Ginkgo* leaves extract was added to solution as ecofriendly fuel agent. The resulting mixture was stirred at constant temperature for 30 min. The obtained products were grinded in an agate mortar to obtain fine powders for further characterizations.

1.2 Characterization techniques

1.2.1. XRD

The powder cobalt-zinc ferrite samples were thoroughly ground in an agate mortar. The powders were applied in even layers on a cuvette with vaseline oil. Experimental intensities and reflection angles were obtained on an automatic diffractometer DRON-2.0M (FeK_α-radiation (Mn filter), angle range 20.00 ≤ 2θ ≤ 130.00°, scanning step is 0.05°; scan time 3 sec/step). The analysis of experimental diffraction patterns and calculations of unit cell parameters were performed using the softwares STOE WinXPOW and PowderCell respectively. The crystal structures was specified by the Rietveld method.

1.2.2. Mössbauer Spectroscopy

Mössbauer spectra were obtained on MS1104Em spectrometer with moving absorber using ⁵⁷Co(Cr) radiation source, the isomeric shift calibrated accordingly to α-Fe. The velocity resolution was about 0.008 mm/s per channel. The obtained signal-to-noise ratios were higher of 31. The Mössbauer spectra were measured at room temperature in transmission geometry.

1.2.3. IR-spectroscopy

Infrared spectra were recorded with a Specord M80 (Carl Zeiss, Germany) spectrophotometer in the range 400-4000 cm⁻¹ (transmission mode). The samples were grinded with KBr in the 1:100 ratio and pressed into

1.1.1. Preparation of *Ginkgo Biloba* leaves extract

The *Ginkgo Biloba* leaves extract was used as “green” reductant. For the preparation of extract, the fresh leaves were boiled with of distilled water (1:2) for 10 minutes and kept out for 24 hours. The filtered extract is stored in a refrigerator at 4-6°C.

1.1.2. Synthesis of Co_{1-x}Zn_xFe₂O₄ NPs

Zn-doped cobalt ferrites were prepared by using sol-gel autocombustion from two types of Me²⁺-containing salts: Co(CH₃COO)₂·4H₂O and Zn(NO₃)₂·6H₂O. As source of ferric ions the iron nitrate Fe(NO₃)₃·9H₂O and *Ginkgo biloba* leaf extract as an effective reducing agent were used. The chemical reactions during the synthesis can be described as follow:

pellets.

1.2.4. Scanning electron microscopy and energy-dispersive spectroscopy

Surface morphology of the samples was studied with a REMMA-102-02 scanning electron microscope (JCS SELMI, Ukraine) with an attachment for energy-dispersive analysis (EDS). The accelerating voltage is approximately 20.00kV.

1.3. Adsorption experiments

The adsorption studies were performed in batch mode. The Congo red dye has been chosen as model dye (Fig. 1) in order to study the adsorption properties of ferrites. 20mg of the adsorbent was inserted in 20 cm³ of a dye solution with a certain concentration (10; 20; 50; 75; 100 mg/L).The mixture was shaken at 25°C and left for 24 hours to establish adsorption equilibrium. The adsorbent were removed using a magnet. The equilibrium concentrations C_e of the dye in the solutions were measured by spectrophotometric method using ULAB-102UV spectrophotometer at a wavelength λ = 510 nm and were determined using the calibration equation. The adsorption capacity (mg/g) was calculated using follow equation:

$$q_{ads} = \frac{(C_0 - C_{eq}) * V}{m}$$

where V is the volume of the solution, L; m is the adsorbent mass, mg; C_e is an equilibrium concentration of CR dye in the solution, mg/L; C₀ is initial concentration of the CR dye in the solution, mg/L. The dye removal (in%) was calculated by the formula:

$$\text{Removal (\%)} = [(C_0 - C_e)/C_0] * 100\%$$

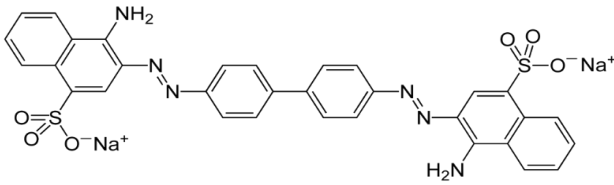


Fig. 1. Chemical structure of azo dye Congo Red (sodium salt of 3,3'-([1,1'-biphenyl]-4,4'-diyl)bis(4-aminonaphthalene-1-sulfonic acid) (IUPAC name: disodium 4-amino-3-[4-[4-(1-amino-4-sulfonato-naphthalen-2-yl)diazenylphenyl]phenyl]diazenyl-naphthalene-1-sulfonate; chemical formula is $C_{32}H_{22}N_6Na_2O_6S_2$; molar mass is 696.665 g/mole).

II. Results and Discussion

2.1. XRD analysis

Spinel structure of synthesized cobalt-zinc ferrites has been confirmed by X-ray analysis (Fig.2) and Rietveld refinement (Fig.3). All cobalt-zinc ferrites are single-phase samples (space group $Fd3m$). It was calculated that the crystallites sizes are in the nanometer range: from 48 nm for cobalt ferrite to 72 nm for zinc ferrite. The increase in Zn content leads to the increase in crystallite sizes. This agrees well with the width of the peaks (Fig. 2). The crystallite size of NPs is obtained from Scherrer formula:

$$D = \frac{0.94 \lambda}{\beta_{1/2} \cos \theta'}$$

where D is average crystallite size; $\beta_{1/2}$ – line broadening (in radians); θ – the angle of (311) peak maximum; $\lambda=0.1936$ nm.

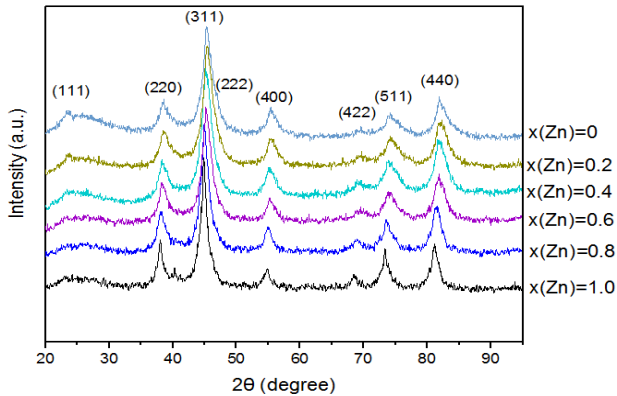


Fig. 2. X-ray diffraction patterns of $Co_{1-x}Zn_xFe_2O_4$ NPs, obtained using Ginkgo Biloba extract.

The calculated crystal parameters (lattice parameter, cell volume, crystallite sizes) and refinement results (reliability factors R_I and R_{WP}) of the spinel $Co_{1-x}Zn_xFe_2O_4$ ferrites, obtained using Ginkgo Biloba extract, are presented in Table 1. It is clear that Zn doping increases the lattice parameter from 8.358 Å for $CoFe_2O_4$ to 8.4343 Å for $ZnFe_2O_4$. The same tendency is observed for cell volume: 584.1 Å³ for $CoFe_2O_4$ to 599.99 Å³ for $ZnFe_2O_4$. The crystallite sizes are increased from 48 Å for $CoFe_2O_4$ to 72 Å for $ZnFe_2O_4$.

The refining results of the spinel structure for the $Co_{1-x}Zn_xFe_2O_4$ samples, obtained using Ginkgo Biloba extract are collected in Table 2. It can be seen that Zn ions placed in tetrahedral positions of the cubic spinel structure, while Co and Fe ions are distributed between the tetrahedral and octahedral positions of the cubic spinel structure. The Rietveld refinement for $Co_{1-x}Zn_xFe_2O_4$ nanoparticles is depicted in Fig. 3. All ferrite samples are single phase and there are no other impurities.

The cation-anion and cation-cation bond lengths had calculated from using the experimental values of lattice constant and oxygen parameter (Table 3) [27,30]. The cation-anion and cation-cation bond lengths for $Co_{1-x}Zn_xFe_2O_4$ nanoparticles are presented in Table 4. It can be seen that Zn ions effect the bond lengths in cobalt ferrite resulting in properties changes.

2.2. Mossbauer spectroscopy

Mossbauer spectra for samples of $Co_{1-x}Zn_xFe_2O_4$ with $x = 0.0, 0.2, 0.4, 0.6, 0.8$ and 1.0 are shown in Fig 5. The spectra show evolution transformation from partially ordered to paramagnetic spin state with an increase in Zn ions concentration. The spectra for $x = 0.0$ show both ordered and paramagnetic behavior at room temperature.

The spectra for $x = 0.2$ shows a doublet and a broad sextet too which is attributed to partially unblocked particles in the state between ferrimagnetic and superparamagnetic. Spectra for $x = 0.4$ demonstrate residual spin relation (background rising) while those for $x = 0.6, 0.8$ and 1.0 shows only paramagnetic behavior. The observation of transition from ordered to paramagnetic spin state is determined by the ratio between the Neel relaxation time τ_N of magnetic moment

Table 1.

Crystal parameters (lattice parameter a , cell volume V , crystallite size D) and refinement results (reliability factors R_I and R_{WP}) of the spinel structure for the $Co_{1-x}Zn_xFe_2O_4$ samples, obtained using Ginkgo Biloba extract.

x	Sample formula	a , Å	V , Å ³	Reliability factors		D , Å
				R_I	R_{WP}	
$x = 0$	$CoFe_2O_4$	8.359(2)	584.1(3)	0.0223	0.0292	48
$x = 0.2$	$Co_{0.8}Zn_{0.2}Fe_2O_4$	8.3629(17)	584.9(2)	0.0155	0.0271	52
$x = 0.4$	$Co_{0.6}Zn_{0.4}Fe_2O_4$	8.3646(16)	585.25(20)	0.0171	0.0263	55
$x = 0.6$	$Co_{0.4}Zn_{0.6}Fe_2O_4$	8.3807(16)	588.64(20)	0.0219	0.0298	60
$x = 0.8$	$Co_{0.2}Zn_{0.8}Fe_2O_4$	8.4018(14)	593.09(17)	0.0242	0.0307	69
$x = 1$	$ZnFe_2O_4$	8.4343(12)	599.99(15)	0.0131	0.0323	72

Table 2.

The refining results of the spinel structure (space group $Fd\bar{3}m$, Pearson symbol $cF56$, $Z=8$) for the $\text{Co}_{1-x}\text{Zn}_x\text{Fe}_2\text{O}_4$ samples, obtained using Ginkgo Biloba extract: atoms coordinates (xyz), parameters of atomic displacement in isotropic approximation (thermal parameters, B_{iso}) and position filling factors G (^{IV}A – cations in tetrahedral positions of the cubic spinel structure, ^{VI}B – cations in octahedral positions of the cubic spinel structure).

Sample	Atoms	Position	$x = y = z$	$B_{iso}, \text{\AA}^2$	G
CoFe_2O_4	^{IV}A	$8a$	0.125	1.17(13)	0.72(2)Fe + 0.28(2)Co
	^{VI}B	$16d$	0.5	1.00(11)	0.639(12)Fe + 0.361(12)Co
	O	$32e$	0.2508(6)	0.98(18)	1
$\text{Co}_{0.8}\text{Zn}_{0.2}\text{Fe}_2\text{O}_4$	^{IV}A	$8a$	0.125	1.02(8)	0.71(4)Fe + 0.09(4)Co + 0.2Zn
	^{VI}B	$16d$	0.5	1.08(7)	0.65(2)Fe + 0.35(2)Co
	O	$32e$	0.2546(4)	1.06(14)	1
$\text{Co}_{0.6}\text{Zn}_{0.4}\text{Fe}_2\text{O}_4$	^{IV}A	$8a$	0.125	1.10(7)	0.57(4)Fe + 0.03(4)Co + 0.4Zn
	^{VI}B	$16d$	0.5	0.99(7)	0.72(2)Fe + 0.28(2)Co
	O	$32e$	0.2550(4)	0.86(13)	1
$\text{Co}_{0.4}\text{Zn}_{0.6}\text{Fe}_2\text{O}_4$	^{IV}A	$8a$	0.125	1.09(8)	0.32(6)Fe + 0.08(6)Co + 0.6Zn
	^{VI}B	$16d$	0.5	0.94(9)	0.84(3)Fe + 0.16(3)Co
	O	$32e$	0.2544(5)	0.57(16)	1
$\text{Co}_{0.2}\text{Zn}_{0.8}\text{Fe}_2\text{O}_4$	^{IV}A	$8a$	0.125	1.24(8)	0.15(6)Fe + 0.05(6)Co + 0.8Zn
	^{VI}B	$16d$	0.5	0.92(9)	0.93(3)Fe + 0.07(3)Co
	O	$32e$	0.2534(6)	0.98(17)	1
ZnFe_2O_4	^{IV}A	$8a$	0.125	1.12(9)	1
	^{VI}B	$16d$	0.5	1.00(10)	1
	O	$32e$	0.2536(8)	0.62(19)	1

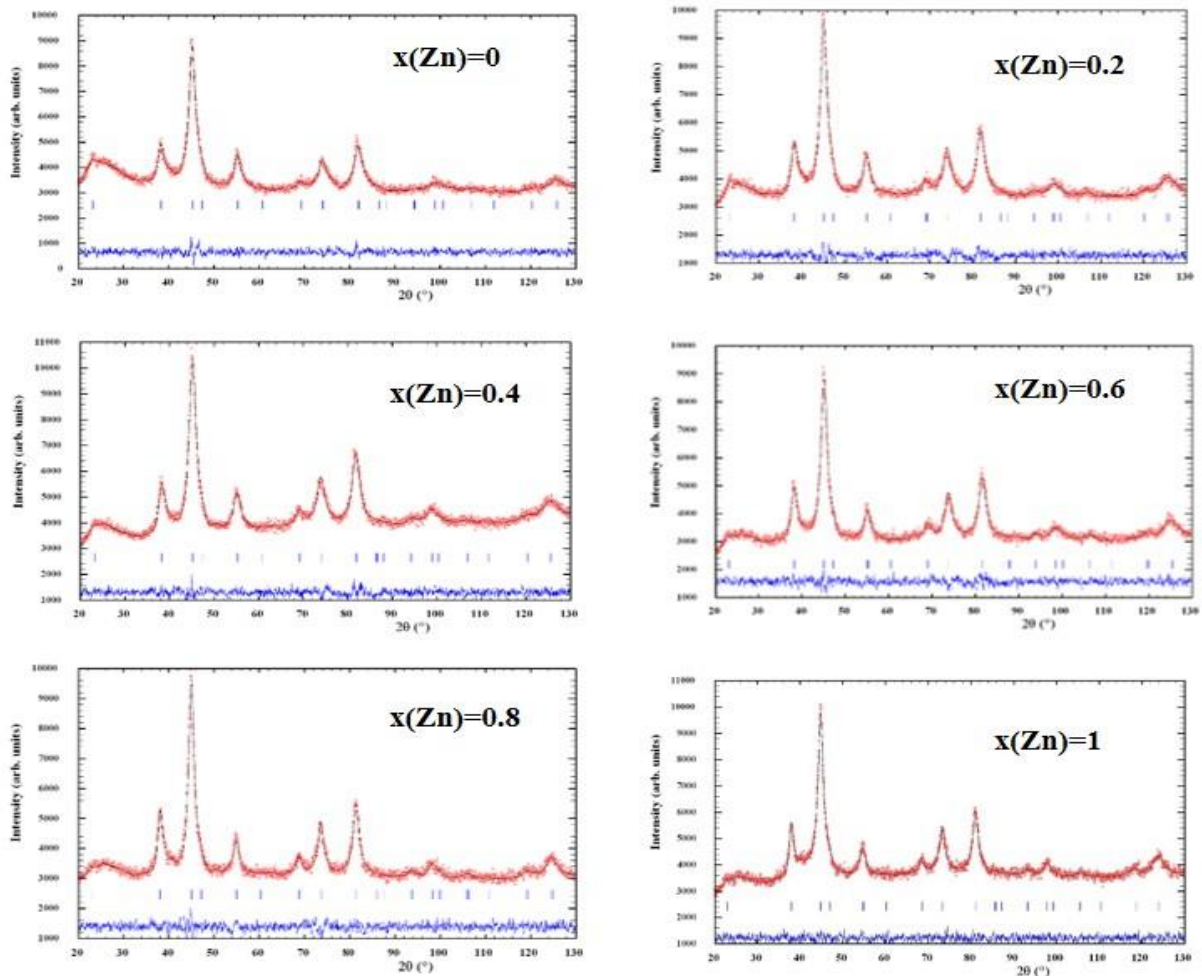


Fig.3. The Rietveld refinement for $\text{Co}_{1-x}\text{Zn}_x\text{Fe}_2\text{O}_4$ nanoparticles.

Table 3.

The formulas used for cation-anion and cation-cation bond lengths calculations.

<i>Me-O:</i>	<i>Me-Me:</i>
$p = a \left(\frac{5}{8} - u \right)$	$b = \sqrt{2} \left(\frac{a}{4} \right)$
$q = a\sqrt{3} \left(u - \frac{1}{4} \right)$	$c = \sqrt{11} \left(\frac{a}{8} \right)$
$r = a\sqrt{11} \left(u - \frac{1}{4} \right)$	$d = \sqrt{3} \left(\frac{a}{4} \right)$
$s = a\sqrt{3} \left(\frac{u}{3} + \frac{1}{8} \right)$	$e = \sqrt{3} \left(\frac{3a}{8} \right)$
	$f = \sqrt{6} \left(\frac{a}{4} \right)$

Table 4.

The cation-anion and cation-cation bond lengths for $\text{Co}_{1-x}\text{Zn}_x\text{Fe}_2\text{O}_4$ NPs.

Parameter	<i>x=0</i>	<i>x=0.2</i>	<i>x=0.4</i>	<i>x=0.6</i>	<i>x=0.8</i>	<i>x=1</i>
u	0.3758	0.3796	0.38	0.3794	0.3784	0.3786
p	2.083	2.052	2.049	2.058	2.071	2.078
q	1.821	1.877	1.883	1.878	1.868	1.878
r	3.487	3.594	3.606	3.596	3.577	3.597
s	3.623	3.643	3.646	3.65	3.655	3.67
b	2.955	2.956	2.957	2.963	2.97	2.982
c	3.465	3.467	3.467	3.474	3.483	3.497
d	3.62	3.621	3.622	3.629	3.638	3.652
e	5.429	5.432	5.433	5.443	5.457	5.478
f	5.119	5.121	5.122	5.132	5.145	5.165

of monodomain nanoparticles and the measurement time τ_m . In a case of Mossbauer spectroscopy method $\tau_m=141.8$ ns as a lifetime of ^{57}Fe nucleus excited state.

Ferrite nanoparticles will be observed at the condition $\frac{\tau_N}{\tau_m} \leq 1$. The Neel time is calculated as

$$\tau_N = \tau_0 \exp\left(\frac{K_{eff} V}{kT}\right),$$

where τ_0 is the characteristic of a material, K_{eff} is a effective magnetocrystalline anisotropy constant, V is a volume of a nanoparticle, T is a temperature, so the particles size decreasing of ferrite with permanent composition typically leads to observation superparamagnetic relaxation of its Mossbauer spectra. However in our case of materials of variable composition the decreasing of the effective anisotropy constant with growth of Zn ions relative content has a greater impact respectively to observed simultaneous particle size increase. The decreasing of a particle size leads to changes of magnetocrystalline anisotropy constant due to cation redistribution with the strong effects of spin canting degree [31].

Magnetocrystalline anisotropy of a mixed ferrite ($\text{Zn}^{2+}_a\text{Co}^{2+}_b\text{Fe}^{3+}_c$)[$\text{Co}^{2+}_d\text{Fe}^{3+}_e$] O_4 ($a+b+d=1$; $c+e=2$) can be calculated as a linear combination of contribution of

the magnetocrystalline anisotropy component of the *all* cations occupied tetrahedral and octahedral sites of spinel structure:

$$K_{eff} = aK_{Zn}^A + bK_{Co}^A + cK_{Fe}^A + dK_{Co}^B + eK_{Fe}^B,$$

where K_i^j – is the contribution of the magnetocrystalline anisotropy of the *i* ion on the *j* site [32]. Accordingly to data presented in [32] the values for the anisotropy contributions for of mixed Co-Zn ferrite particles are:

$$\begin{aligned} K_{Zn}^A &= 0, \\ K_{Co}^A &= 7.66 \cdot 10^5 \text{ J/m}^3, \\ K_{Fe}^A &= -1.18 \cdot 10^6 \text{ J/m}^3, \\ K_{Co}^B &= 1.07 \cdot 10^6 \text{ J/m}^3, \\ K_{Fe}^B &= 1.78 \cdot 10^5 \text{ J/m}^3 \end{aligned}$$

The calculated using this approach values of magnetocrystalline anisotropy re shown in Table 5.

Magnetocrystalline anisotropy of non-substituted CoFe_2O_4 varied dependently to material stoichiometry in a range from $2.1 \cdot 10^5$ to $3.9 \cdot 10^5$ J/m^3 at 300 K [33] so the obtained value of $K_{eff}=3.63 \cdot 10^5$ J/m^3 is very realistic.

The surface anisotropy formed by a disordered

Table 5.

The values for the anisotropy contributions for $\text{Co}_{1-x}\text{Zn}_x\text{Fe}_2\text{O}_4$ NPs.

Sample	Cation distribution	K_{eff}
CoFe_2O_4	$(\text{Co}^{2+}_{0.28} \text{Fe}^{3+}_{0.72})[\text{Co}^{2+}_{0.72} \text{Fe}^{3+}_{1.28}]\text{O}_4$	$3.63 \cdot 10^5$
$\text{Co}_{0.8}\text{Zn}_{0.2}\text{Fe}_2\text{O}_4$	$(\text{Zn}^{2+}_{0.18} \text{Co}^{2+}_{0.09} \text{Fe}^{3+}_{0.73})[\text{Zn}^{2+}_{0.02} \text{Co}^{2+}_{0.70} \text{Fe}^{3+}_{1.28}]\text{O}_4$	$2.12 \cdot 10^5$
$\text{Co}_{0.6}\text{Zn}_{0.4}\text{Fe}_2\text{O}_4$	$(\text{Zn}^{2+}_{0.31} \text{Co}^{2+}_{0.03} \text{Fe}^{3+}_{0.66})[\text{Zn}^{2+}_{0.09} \text{Co}^{2+}_{0.56} \text{Fe}^{3+}_{1.35}]\text{O}_4$	$2.06 \cdot 10^5$
$\text{Co}_{0.4}\text{Zn}_{0.6}\text{Fe}_2\text{O}_4$	$(\text{Zn}^{2+}_{0.39} \text{Co}^{2+}_{0.08} \text{Fe}^{3+}_{0.53})[\text{Zn}^{2+}_{0.21} \text{Co}^{2+}_{0.32} \text{Fe}^{3+}_{1.47}]\text{O}_4$	$3.99 \cdot 10^4$
$\text{Co}_{0.2}\text{Zn}_{0.8}\text{Fe}_2\text{O}_4$	$(\text{Zn}^{2+}_{0.56} \text{Co}^{2+}_{0.05} \text{Fe}^{3+}_{0.39})[\text{Zn}^{2+}_{0.24} \text{Co}^{2+}_{0.14} \text{Fe}^{3+}_{1.62}]\text{O}_4$	$1.63 \cdot 10^4$
ZnFe_2O_4	$(\text{Zn}^{2+}_{0.74} \text{Fe}^{3+}_{0.26})[\text{Zn}^{2+}_{0.26} \text{Fe}^{3+}_{1.74}]\text{O}_4$	$2.92 \cdot 10^3$

surface spins layer and also interparticle interactions between neighbouring nanoparticles increase the K_{eff} values of ultrafine ferrites [34].

The data presented in [35] were fitted with Boltzmann sigmoidal function that allow to obtain the analytical dependence between K_{eff} of nanosized mixed Co-Zn spinel ferrite and Zn content. Using this dependence the values of K_{eff} for investigated system of sample were calculated for each value of Zn relative content (Fig.4).

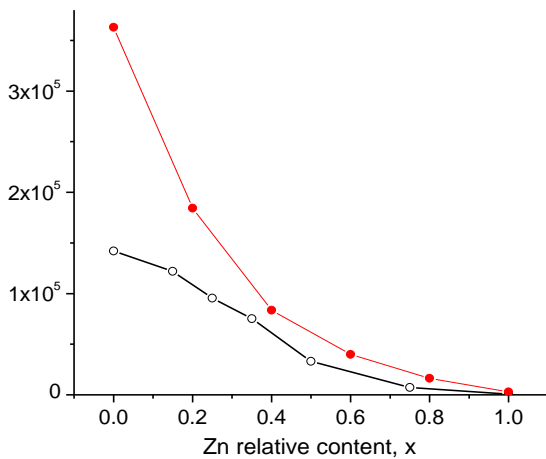


Fig.4. The analytical dependence between K_{eff} of nanosized mixed Co-Zn spinel ferrite and Zn content.

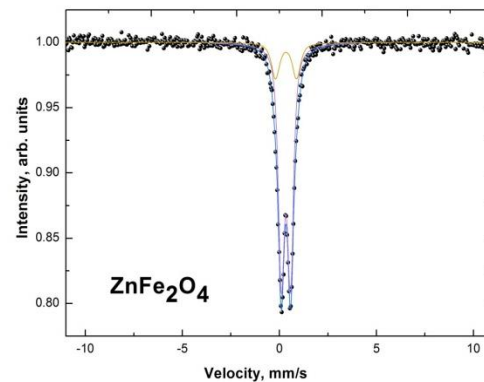
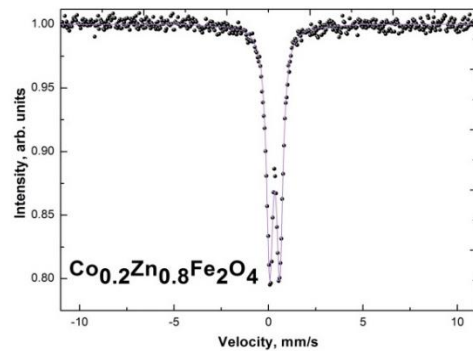
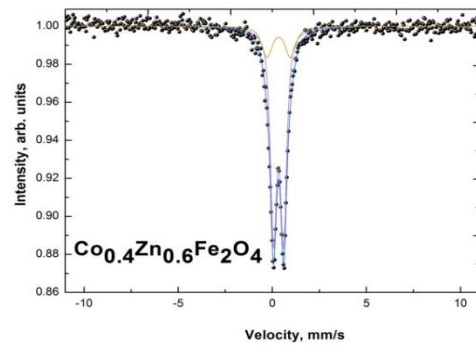
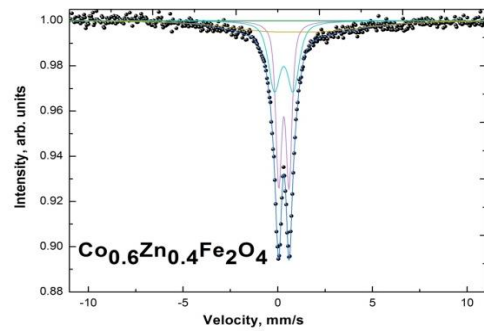
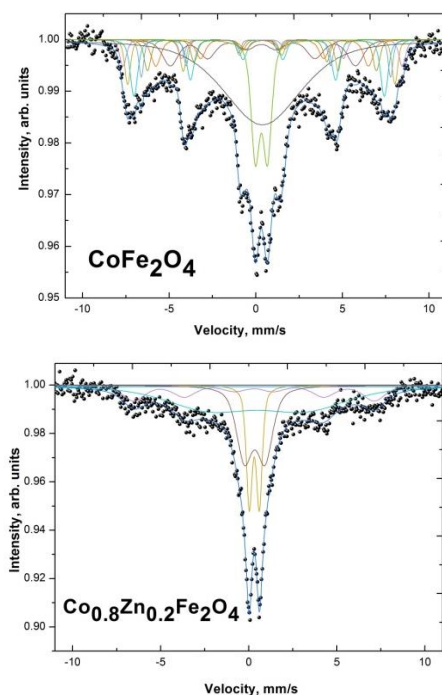


Fig.5. Mossbauer spectra of $\text{Co}_{1-x}\text{Zn}_x\text{Fe}_2\text{O}_4$ NPs, synthesized using Ginkgo Biloba extract.

2.3. Scanning Electron Microscopy (SEM)

SEM images of $\text{Co}_{1-x}\text{Zn}_x\text{Fe}_2\text{O}_4$ ($0 \leq x < 1.0$ with step 0.2) samples are presented in Fig.6. Samples with $x(\text{Zn})=0$ to $x(\text{Zn})=0.2$ are more porous than samples with $x(\text{Zn})$ from 0.4 to 1.0. The particles agglomerates are mostly spherical. The surface of the samples with $x(\text{Zn})$

from 0.6 to 1.0 reveal strong tendency to agglomerations. Energy dispersive spectroscopy (EDS) spectra of samples confirm the presence of O, Fe Co and Zn elements (Table 6). The elemental composition of all samples is correlated to the stoichiometric theoretical composition of cobalt-zinc ferrites.

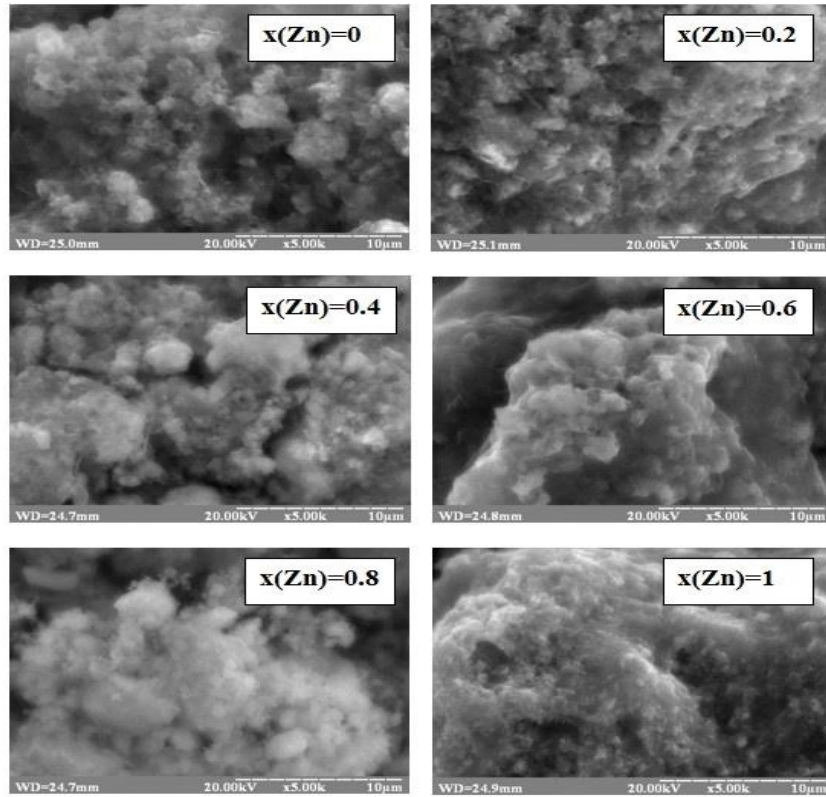


Fig.6. SEM images of $\text{Co}_{1-x}\text{Zn}_x\text{Fe}_2\text{O}_4$ NPs synthesized using Ginkgo Biloba extract.

Table 6.

Chemical composition of $\text{Co}_{1-x}\text{Zn}_x\text{Fe}_2\text{O}_4$ NPs due to EDS data.

Sample	Element	at. %	wt. %
CoFe_2O_4	O	57.17	27.57
	Fe	28.68	49.94
	Co	14.15	22.49
$\text{Zn}_{0.2}\text{Co}_{0.8}\text{Fe}_2\text{O}_4$	O	57.07	27.04
	Fe	28.26	46.74
	Co	11.54	20.15
	Zn	3.13	6.07
$\text{Zn}_{0.4}\text{Co}_{0.6}\text{Fe}_2\text{O}_4$	O	57.08	26.92
	Fe	28.33	46.64
	Co	8.8	15.29
	Zn	5.79	11.15
$\text{Zn}_{0.6}\text{Co}_{0.4}\text{Fe}_2\text{O}_4$	O	57.07	26.71
	Fe	28.28	46.13
	Co	5.62	9.04
	Zn	9.03	18.12
$\text{Zn}_{0.8}\text{Co}_{0.2}\text{Fe}_2\text{O}_4$	O	57.09	26.6
	Fe	28.35	46.09
	Co	2.22	3.81
	Zn	12.34	23.49
ZnFe_2O_4	O	57.05	26.44
	Fe	28.20	45.63
	Zn	14.74	27.93

2.4. IR spectroscopy

IR spectra of synthesized sample shown the presence of spinel structure (Fig.7). The two bands of the absorption peaks prove the formation of spinel structure. The band at 416-360 cm⁻¹ is characteristic to the M-O vibration of ions located in octahedral sites. The strong band at 552-604 cm⁻¹ is characteristic to vibration of M-O ions located in tetrahedral sites. The peak in the 1120 cm⁻¹ shows the presence of deformation vibrations of organic -CH₂ group, derived from green extract used for spinels synthesis.

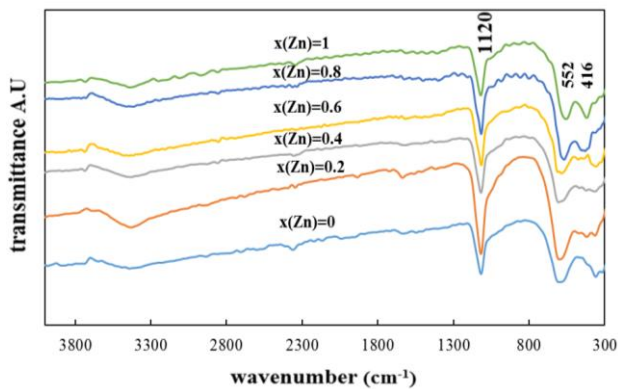


Fig.7. The FT-IR spectra of spinel $\text{Co}_{1-x}\text{Zn}_x\text{Fe}_2\text{O}_4$ samples.

2.5. Adsorption properties

The obtained ferrites were examined as magnetic adsorbents using Congo Red (CR) dye as model pollutant (Fig.8). The main factors affecting the adsorption of dye molecules are the solution pH, the molecules structure and the nature of the active surface centers. The efficiency of CR dye adsorption increased with zinc content increasing from $x(\text{Zn})=0$ to $x(\text{Zn})=0.4$. The sample $\text{Co}_{0.6}\text{Zn}_{0.4}\text{Fe}_2\text{O}_4$ demonstrate the best adsorption properties towards CR removal ($q_{\text{ads}}= 53.08 \text{ mg/g}$). The obtained adsorption isotherms were analyzed using Langmuir and Freundlich models (Fig.9).

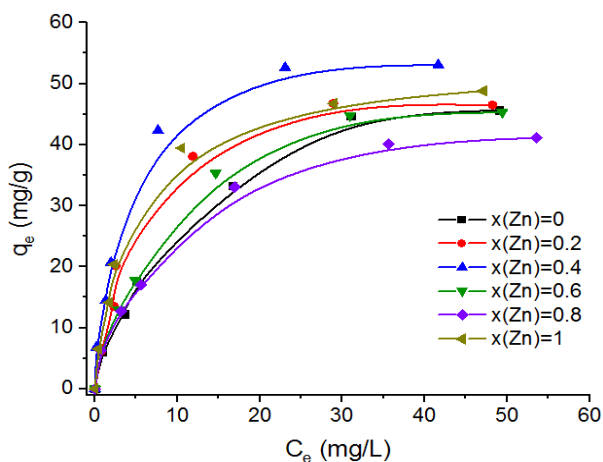


Fig. 8. Isotherms of the Congo Red dye adsorption from the aqueous solutions using cobalt-zinc ferrites.

Langmuir model describe adsorption processes on the adsorbent [4]. According to this theory, adsorption

takes place at specific homogeneous sites inside the adsorbent. These sites are called active centers. After the dye molecule moves deeper into the adsorbent, the adsorption takes place at the active centers of the adsorbent [36]. According to the Langmuir model, the adsorption is carried out with the participation of adsorption centers on the surface; those centers interact only with one molecule of the adsorbate and, as a result, form a monomolecular layer. The eq. (1) describes the linear expression of the Langmuir isotherm:

$$\frac{C_e}{q_e} = \left(\frac{1}{q_{\text{max}}} \right) C_e + \frac{1}{q_{\text{max}} K_L} \quad (1)$$

where q_e is the amount of adsorbed Congo red dye per 1 g of adsorbent at equilibrium adsorption (mg/g); q_{max} is the maximum adsorption capacity of the monolayer at saturation (mg/g); C_e is the Congo red dye concentration at equilibrium point (mg/L); K_L is a Langmuir equilibrium constant that takes into account all interactions in the solution (L/mg). Thus, a plot of C_e/q_e vs. C_e gives the magnitudes of q_m and K_L . The calculated results are presented in Table 8. A separation factor R_L has been calculated from eq. (2):

$$R_L = \frac{1}{1 + K_L C_0} \quad (2)$$

where K_L (L/mg) is the Langmuir constant, C_0 (mg/L) is the initial Congo red dye amount. The separation factor R_L gives us the information about adsorption: linear ($R_L = 1$), unfavorable ($R_L > 1$), favorable ($0 < R_L < 1$), or irreversible ($R_L = 0$). It was concluded (Table S1) that $0 < R_L < 1$, what means the samples are favorable for Congo red dye adsorption.

The Freundlich equilibrium isotherm was also used to describe adsorption processes on our experimental samples. The Freundlich theory describes adsorption processes with a uniform energy distribution of heterogeneous surface. The application of the Freundlich equation suggests that adsorption energy exponentially decreases on completion of the adsorption centers of an adsorbent. The linear form of Freundlich theory can be represented as follows:

$$\log q_e = \frac{1}{n} \log C_e + \log K_F \quad (3)$$

where K_F is Freundlich constant; $1/n$ is a parameter, indicating the intensity of the adsorbent-adsorbate interaction [4].

Linearized adsorption isotherms of Congo red dye on the cobalt-zinc ferrites surface are shown in Fig. 9a and 9b. The comparison of the determination coefficients concludes that the linear equations obtained by the Langmuir model are characterized by higher R^2 values. The calculated values of the constants of the Langmuir and Freundlich equations for the adsorption isotherms of Congo red dye on six ferrite samples are given in Table 8.

Table 7.

IR absorption bands of $\text{Co}_{1-x}\text{Zn}_x\text{Fe}_2\text{O}_4$ samples.

Parameters	x(Zn)=0	x(Zn)=0.2	x(Zn)=0.4	x(Zn)=0.6	x(Zn)=0.8	x(Zn)=1
ν_T, cm^{-1}	604	600	604	580	568	552
ν_O, cm^{-1}	360	368	368	356	432	416

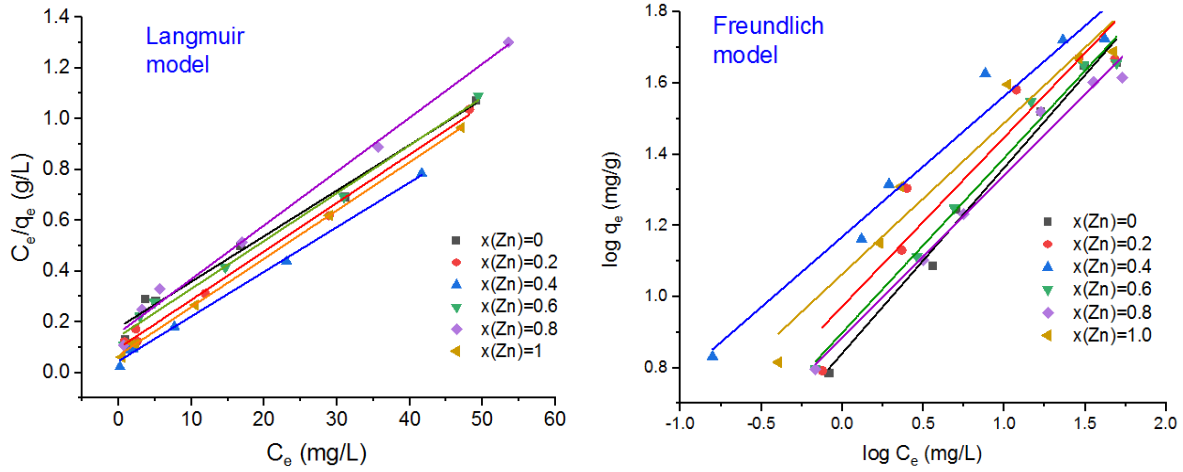


Fig. 9. Linearized adsorption isotherms of Congo red dye on the cobalt-zinc ferrites surface according to Langmuir and Freundlich models.

Table 8.

The parameters of Langmuir and Freundlich adsorption models.

Sample	$q_{\text{exp}}, \text{mg/g}$	Adsorption model						
		Langmuir				Freundlich		
		R_L	K_L	q_{max}	R^2	K_F	n	R^2
CoFe_2O_4	45.7	0.09	0.099	55.87	0.985	6.9	1.92	0.985
$\text{Co}_{0.8}\text{Zn}_{0.2}\text{Fe}_2\text{O}_4$	46.5	0.05	0.197	52.4	0.996	9.4	2.11	0.996
$\text{Co}_{0.6}\text{Zn}_{0.4}\text{Fe}_2\text{O}_4$	53.08	0.03	0.377	56.82	0.997	14.7	2.53	0.997
$\text{Co}_{0.4}\text{Zn}_{0.6}\text{Fe}_2\text{O}_4$	45.3	0.07	0.132	53.19	0.990	7.9	2.04	0.990
$\text{Co}_{0.2}\text{Zn}_{0.8}\text{Fe}_2\text{O}_4$	41.2	0.07	0.135	47.17	0.992	7.7	2.2	0.992
ZnFe_2O_4	48.8	0.04	0.274	52.63	0.999	11.6	2.35	0.999

From the Table 8 it follows that the Langmuir constant K_L increases with the Zn content increasing. The Langmuir constant characterizes the energy of the interaction of adsorbate with the adsorbent. The stronger this interaction, the greater the value of the adsorption constant. The Langmuir constant K_L is highest for the $\text{Co}_{0.6}\text{Zn}_{0.4}\text{Fe}_2\text{O}_4$ sample and lowest for the $\text{Co}_{0.4}\text{Zn}_{0.6}\text{Fe}_2\text{O}_4$ and $\text{Co}_{0.2}\text{Zn}_{0.8}\text{Fe}_2\text{O}_4$ samples. It is seen that the incorporation of Zn in cobalt ferrite also leads to an increase in the interaction of CR dye molecules with the adsorbent surface until $x(\text{Zn})=0.4$. Consequently, the energy of interaction between CR dye and the adsorbent surface firstly increases when Zn content increases. From the data of Table 8 it follows that the Freundlich constant K_F is highest for the $\text{Co}_{0.6}\text{Zn}_{0.4}\text{Fe}_2\text{O}_4$ sample and lowest for the CoFe_2O_4 sample. The increase in Zn content leads to an increase in the interaction of CR dye molecules with the adsorbent surface. For samples $\text{Co}_{0.4}\text{Zn}_{0.6}\text{Fe}_2\text{O}_4$ and $\text{Co}_{0.2}\text{Zn}_{0.8}\text{Fe}_2\text{O}_4$ the K_F values are comparable. The Freundlich model is used to describe adsorption on non-uniform surfaces. According to this model, the adsorption centers have different energies, and the

binding of Congo red dye molecules with of the most active adsorption centers with the maximum adsorption energy onto ferrite surface occurs first of all. The applicability of the Freundlich model to the description of the Congo red dye adsorption may indicate the inhomogeneity of the adsorbents surface. There are active surface centers with different adsorption energy and the adsorption of CR dye molecules going unevenly.

Taking into account the CR dye molecular structure it could be concluded that the adsorption of CR dye occurs on the active surface centers of the adsorbents, charged positively. The interaction between positively charged active centers and the surface of the adsorbent proceeds according to the donor-acceptor mechanism. We assume that the ferric ions Fe_A^{3+} , placed in the tetrahedral sites of spinel structure, are the positively charged active centers according to the antistructure modeling. The percentage of Congo red dye removal from water solutions by cobalt-zinc ferrites presented in Fig. 10.

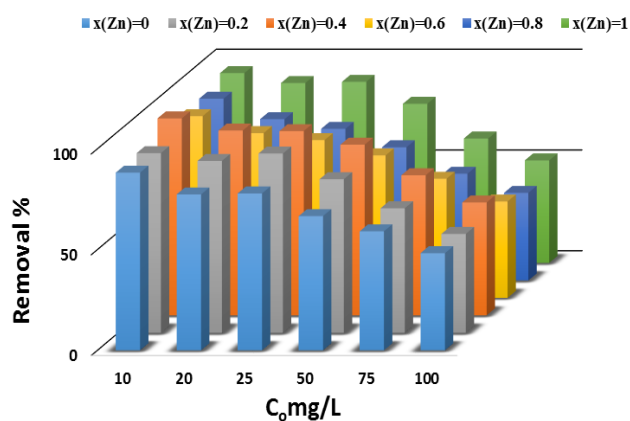


Fig. 10. Removal of Congo red dye from water solutions by cobalt-zinc ferrites.

Conclusions

Cobalt ferrite nanopowders were successfully synthesized by means of the green method, using *Ginkgo biloba* leaf extract as a eco-friendly fuel agent and reductant. The spinel structure was studied by the X-ray analysis and confirmed by the Mossbauer spectroscopy. Structural characteristics of adsorbents have been determined. The surface morphology were characterized by SEM, which revealed a homogenous microstructure. The elemental composition were analyzed by EDS. Adsorption properties of cobalt-zinc ferrites were investigated using Congo Red dye as model pollutant. The adsorption isotherms were obtained in the batch mode. The adsorption isotherms were fitted by

using Langmuir and Freundlich models. It is shown that an increase in the zinc content leads to an increase in the adsorption of the CR dye up to $x(\text{Zn})=0.4$. The $\text{Co}_0.6\text{Zn}_0.4\text{Fe}_2\text{O}_4$ sample with demonstrated the best adsorption activity. The changes in adsorption capacities could be associated with changes in the number of active surface centers with which the CR dye molecules could interact.

Acknowledgement

The authors thank the Ministry of Education and Science of Ukraine for financial support in the framework of project number 0121U109476 ("Engineering of metal oxide catalysts with the regulating activity function for hydroxyradical water disinfection", 2021-2023).

Liaskovska Mariia – graduate student of Chemistry Department Vasyl Stefanyk Precarpathian National University, assistant at Ivano-Frankivsk National Medical University

Tetiana Tatarchuk – Associate Professor of the Chemistry Department, Director of Educational and Scientific Center of Material Science and Nanotechnology, Vasyl Stefanyk Precarpathian National University;

Volodymyr Kotsyubynsky - Doctor of Physical and Mathematical Sciences, Vasyl Stefanyk Precarpathian National University;

Ersteniuk Hanna - Doctor of Biological Sciences, Professor, Ivano-Frankivsk National Medical University.

- [1] F. Buazar, M.H. Baghlani-Nejzad, M. Badri, M. Kashisaz, A. Khaledi-Nasab, F. Kroushawi, Facile one-pot phytosynthesis of magnetic nanoparticles using potato extract and their catalytic activity, *Starch/Staerke*. 68, 796–804 (2016); <https://doi.org/10.1002/star.201500347>.
- [2] K. Kombaiah, J.J. Vijaya, L.J. Kennedy, M. Bououdina, R.J. Ramalingam, H.A. Al-Lohedan, Comparative investigation on the structural, morphological, optical, and magnetic properties of CoFe_2O_4 nanoparticles, *Ceram. Int.* 43, 7682–7689 (2017); <https://doi.org/10.1016/j.ceramint.2017.03.069>.
- [3] N. Ghazi, H. Mahmoudi Chenari, F.E. Ghodsi, Rietveld refinement, morphology analysis, optical and magnetic properties of magnesium-zinc ferrite nanofibers, *J. Magn. Magn. Mater.* (2018); <https://doi.org/10.1016/j.jmmm.2018.07.084>.
- [4] M. Iram, C. Guo, Y. Guan, A. Ishfaq, H. Liu, Adsorption and magnetic removal of neutral red dye from aqueous solution using Fe_3O_4 hollow nanospheres, *J. Hazard. Mater.* 181, 1039–1050 (2010); <https://doi.org/10.1016/j.jhazmat.2010.05.119>.
- [5] J. Gilabert, M.D. Palacios, V. Sanz, S. Mestre, Fuel effect on solution combustion synthesis of $\text{Co}(\text{Cr},\text{Al})_2\text{O}_4$ pigments, *Bol. La Soc. Esp. Ceram. y Vidr.* 56, 215–225 (2017); <https://doi.org/10.1016/j.bsecv.2017.03.003>.
- [6] B.I. Kharisov, H.V.R. Dias, O. V. Kharissova, Mini-review: Ferrite nanoparticles in the catalysis, *Arab. J. Chem.* (2019); <https://doi.org/10.1016/j.arabjc.2014.10.049>.
- [7] C. Li, X. Han, F. Cheng, Y. Hu, C. Chen, J. Chen, Phase and composition controllable synthesis of cobalt manganese spinel nanoparticles towards efficient oxygen electrocatalysis, *Nat. Commun.* 6, 1–8 (2015); <https://doi.org/10.1038/ncomms8345>.
- [8] H. Liu, A. Li, X. Ding, F. Yang, K. Sun, Magnetic induction heating properties of $\text{Mg}_{1-x}\text{Zn}_x\text{Fe}_2\text{O}_4$ ferrites synthesized by co-precipitation method, *Solid State Sci.* 93 (2019); <https://doi.org/10.1016/j.solidstatesciences.2019.05.005>.
- [9] K. Hedayati, S. Azarakhsh, D. Ghanbari, Synthesis and magnetic investigation of cobalt ferrite nanoparticles prepared via a simple chemical precipitation method, *J. Nanostruct.* 6, 127–131 (2016); <https://doi.org/10.7508/jns.2016.02.004>.

- [10] T. Tatarchuk, N. Paliychuk, R.B. Bitra, A. Shyichuk, M.U. Naushad, I. Mironyuk, D. Ziółkowska, Adsorptive removal of toxic methylene blue and acid orange 7 dyes from aqueous medium using cobalt-zinc ferrite nanoadsorbents, *Desalin. Water Treat.* (2019); <https://doi.org/10.5004/dwt.2019.23751>.
- [11] Z. Chen, E. Shi, W. Li, Y. Zheng, W. Zhong, Hydrothermal synthesis and optical property of nano-sized CoAl₂O₄ pigment, *Mater. Lett.* 55, 281–284 (2002); [https://doi.org/10.1016/S0167-577X\(02\)00378-6](https://doi.org/10.1016/S0167-577X(02)00378-6).
- [12] R. Naghikhani, G. Nabiyouni, D. Ghanbari, Simple and green synthesis of CuFe₂O₄–CuO nanocomposite using some natural extracts: photo-degradation and magnetic study of nanoparticles, *J. Mater. Sci. Mater. Electron.* 29, 4689–4703 (2018); <https://doi.org/10.1007/s10854-017-8421-1>.
- [13] B.G. Toksha, S.E. Shirsath, S.M. Patange, K.M. Jadhav, Structural investigations and magnetic properties of cobalt ferrite nanoparticles prepared by sol-gel auto combustion method, *Solid State Commun.* 147, 479–483 (2008); <https://doi.org/10.1016/j.ssc.2008.06.040>.
- [14] Q. Tang, H. Zhu, C. Chen, Y. Wang, Z. Zhu, J. Wu, W. Shih, Preparation and characterization of nanoscale cobalt blue pigment for ceramic inkjet printing by sol-gel self-propagating combustion, *Mater. Res.* 20, 1340–1344 (2017); <https://doi.org/10.1590/1980-5373-MR-2017-0322>.
- [15] J.R.C. Proveti, P.S.S. Porto, E.P. Muniz, R.D. Pereira, D.R. Araujo, M.B. Silveira, Sol–gel proteic method using orange albedo pectin for obtaining cobalt ferrite particles, *J. Sol-Gel Sci. Technol.* 75, 31–37 (2015); <https://doi.org/10.1007/s10971-015-3671-y>.
- [16] P.Y. Reyes-Rodríguez, D.A. Cortés-Hernández, J.C. Escobedo-Bocardo, J.M. Almanza-Robles, H.J. Sánchez-Fuentes, A. Jasso-Terán, L.E. De León-Prado, J. Méndez-Nonell, G.F. Hurtado-López, Structural and magnetic properties of Mg–Zn ferrites (Mg_{1-x}Zn_xFe₂O₄) prepared by sol-gel method, *J. Magn. Magn. Mater.* 427 (2017); <https://doi.org/10.1016/j.jmmm.2016.10.078>.
- [17] M.C.G. Merino, A.L. Estrella, M.E. Rodríguez, L. Acuña, M.S. Lassa, G.E. Lascalea, P. Vázquez, Combustion Syntheses of CoAl₂O₄ Powders Using Different Fuels, *Procedia Mater. Sci.* 8, 519–525 (2015); <https://doi.org/10.1016/j.mspro.2015.04.104>.
- [18] P. Vlazan, M. Stoia, Structural and magnetic properties of CoFe₂O₄ nanopowders, prepared using a modified Pechini method, *Ceram. Int.* 44, 530–536 (2018); <https://doi.org/10.1016/j.ceramint.2017.09.207>.
- [19] V.C. Karade, T.D. Dongale, S.C. Sahoo, P. Kollu, A.D. Chougale, P.S. Patil, P.B. Patil, Effect of reaction time on structural and magnetic properties of green-synthesized magnetic nanoparticles, *J. Phys. Chem. Solids.* 120, 161–166 (2018); <https://doi.org/10.1016/j.jpcs.2018.04.040>.
- [20] H. Hwang, H. Shin, W.J. Lee, Effects of calcination temperature for rate capability of triple-shelled ZnFe₂O₄ hollow microspheres for lithium ion battery anodes, *Sci. Rep.* 7, 1–10 (2017); <https://doi.org/10.1038/srep46378>.
- [21] I.M. Chung, I. Park, K. Seung-Hyun, M. Thiruvengadam, G. Rajakumar, Plant-Mediated Synthesis of Silver Nanoparticles: Their Characteristic Properties and Therapeutic Applications, *Nanoscale Res. Lett.* 11, 1–14 (2016); <https://doi.org/10.1186/s11671-016-1257-4>.
- [22] S. Gómez-Graña, M. Perez-Ameneiro, X. Vecino, I. Pastoriza-Santos, J. Perez-Juste, J.M. Cruz, A.B. Moldes, Biogenic synthesis of metal nanoparticles using a biosurfactant extracted from corn and their antimicrobial properties, *Nanomaterials.* 7 (2017); <https://doi.org/10.3390/nano7060139>.
- [23] M. Liaskovska, T. Tatarchuk, M. Bououdina, I. Mironyuk, Green Synthesis of Magnetic Spinel Nanoparticles, in: *Springer Proc. Phys.*, (2019); https://doi.org/10.1007/978-3-030-17755-3_25.
- [24] P. Laokul, V. Amornkitbamrung, S. Seraphin, S. Maensiri, Characterization and magnetic properties of nanocrystalline CuFe₂O₄, NiFe₂O₄, ZnFe₂O₄ powders prepared by the Aloe vera extract solution, *Curr. Appl. Phys.* 11, 101–108 (2011); <https://doi.org/10.1016/j.cap.2010.06.027>.
- [25] B.S. Surendra, M. Veerabhadrswamy, K.S. Anantharaju, H.P. Nagaswarupa, S.C. Prashantha, Green and chemical-engineered CuFe₂O₄: characterization, cyclic voltammetry, photocatalytic and photoluminescent investigation for multifunctional applications, *J. Nanostructure Chem.* 8, 45–59 (2018); <https://doi.org/10.1007/s40097-018-0253-x>.
- [26] K. Kombaiah, J.J. Vijaya, L.J. Kennedy, M. Bououdina, R.J. Ramalingam, H.A. Al-Lohedan, Okra extract-assisted green synthesis of CoFe₂O₄ nanoparticles and their optical, magnetic, and antimicrobial properties, *Mater. Chem. Phys.* 204, 410–419 (2018); <https://doi.org/10.1016/j.matchemphys.2017.10.077>.
- [27] T. Tatarchuk, M. Liaskovska, V. Kotsyubynsky, M. Bououdina, Green synthesis of cobalt ferrite nanoparticles using *Cydonia oblonga* extract: structural and mössbauer studies, *Mol. Cryst. Liq. Cryst.* 672 (2018); <https://doi.org/10.1080/15421406.2018.1542107>.
- [28] M. Liaskovska, T. Tatarchuk, Green synthesis of zinc ferrite, *Mol. Cryst. Liq. Cryst.* 719, 45–52 (2021); <https://doi.org/10.1080/15421406.2020.1862459>.
- [29] J.W. Han, J. Kim, J. Kim, IJN-53538-ginkgo-biloba--a-natural-reducing-agent-for-the-synthesis-of_010714, 363–377 (2014).
- [30] T.R. Tatarchuk, M. Bououdina, N.D. Paliychuk, I.P. Yaremiy, V. V. Moklyak, Structural characterization and antistructure modeling of cobalt-substituted zinc ferrites, *J. Alloys Compd.* 694, 777–791 (2017); <https://doi.org/10.1016/j.jallcom.2016.10.067>.
- [31] A. Omelyanchik, M. Salvador, F. D’orazio, V. Mameli, C. Cannas, D. Fiorani, A. Musinu, M. Rivas, V. Rodionova, G. Varvaro, D. Peddis, Magnetocrystalline and surface anisotropy in coFe₂O₄ nanoparticles, *Nanomaterials.* 10, 1–11 (2020); <https://doi.org/10.3390/nano10071288>.

- [32] L.H.G. De Biasi, R. S., & Cardoso, A simple model for the magnetocrystalline anisotropy in mixed ferrite nanoparticles, *Phys. B Condens. Matter.* 407 (2012); <https://doi.org/https://www.sciencedirect.com/science/article/pii/S0921452612006369>.
- [33] N. Ranvah, Y. Melikhov, D.C. Jiles, J.E. Snyder, A.J. Moses, P.I. Williams, S.H. Song, Temperature dependence of magnetic anisotropy of Ga-substituted cobalt ferrite, in: *J. Appl. Phys.* (2008); <https://doi.org/10.1063/1.2832503>.
- [34] and J.P.L. Mohapatra, Jeotikanta, Meiyong Xing, Inductive thermal effect of ferrite magnetic nanoparticles, *Materials* (Basel) (2019).
- [35] A. Omelyanchik, K. Levada, S. Pshenichnikov, M. Abdolrahim, M. Baricic, A. Kapitonova, A. Galieva, S. Sukhikh, L. Astakhova, S. Antipov, B. Fabiano, D. Peddis, V. Rodionova, Green synthesis of co-zn spinel ferrite nanoparticles: Magnetic and intrinsic antimicrobial properties, *Materials* (Basel). 13, 1–13 (2020); <https://doi.org/10.3390/ma13215014>.
- [36] S.J. Allen, Q. Gan, R. Matthews, P.A. Johnson, Comparison of optimised isotherm models for basic dye adsorption by kudzu, *Bioresour. Technol.* (2003); [https://doi.org/10.1016/S0960-8524\(02\)00281-X](https://doi.org/10.1016/S0960-8524(02)00281-X).

Марія Лясковська^{1,2}, Тетяна Татарчук³, Володимир Коцюбинський⁴,
Ганна Ерстенюк²

Zn-заміщені наночастинки CoFe₂O₄, синтезовані з використанням екстракту Гінкго Білоби: катіонний розподіл, мессбауерівські дослідження та застосування для очищення води

¹ Кафедра хімії, Прикарпатський національний університет імені Василя Стефаника, вул. Шевченка 57, Івано-Франківськ, 76018, Україна liaskovskam@gmail.com

² Кафедра біологічної та медичної хімії імені академіка Г.О. Бабенка, Івано-Франківський національний медичний університет, вул. Галицька 2, Івано-Франківськ, 76018, Україна erst@ukr.net

³ Навчально-науковий центр хімічного матеріалознавства та нанотехнологій, Прикарпатський національний університет імені Василя Стефаника, вул. Галицька 201, Івано-Франківськ, Україна 201, tatarchuk.tetyana@gmail.com

⁴ Кафедра матеріалознавства і новітніх технологій, Прикарпатський національний університет імені Василя Стефаника, вул. Шевченка 57, Івано-Франківськ, 76018, Україна, kotsuybynsky@gmail.com

Кобальт-цинкові ферити складу Zn_{1-x}Co_xFe₂O₄ (де x=0; 0,2; 0,4; 0,6; 0,8; 1,0) отримано методом «зеленого синтезу» з використанням екстракту листа Гінкго Білоби як відновника. Методами X-променевої дифракції та мессбауерівської спектроскопії досліджено розподіл катіонів шпінельних феритів. Морфологію поверхні та елементний склад проаналізовано за допомогою СЕМ та ЕДС. Розмір кристалітів, розрахований за формулою Шеррера та методом Вільямсона-Холла, зменшується із збільшенням вмісту Co²⁺. Адсорбційні властивості шпінельних наночастинок досліджено по відношенню до барвника Конго червоного як модельного забруднювача. Встановлено, що адсорбція молекул барвника Конго червоного може відбуватися за рахунок електростатичної та донорно-акцепторної взаємодії з поверхнею адсорбенту, яка містить різну кількість активних центрів.

Ключові слова: кобальтовий ферит; шпінель; зелений синтез; адсорбція; барвник.